Journal of Power Sources 198 (2012) 83–89

Contents lists available at SciVerse ScienceDirect

Journal of Power Sources

journal homepage: www.elsevier.com/locate/jpowsour

The use of carbon nanotubes coated with a porous nitrogen-doped carbon layer with embedded Pt for the methanol oxidation reaction

Chun-Han Hsu, Ping-Lin Kuo*

Department of Chemical Engineering, National Cheng Kung University, Tainan 70101, Taiwan, ROC

ARTICLE INFO

Article history:
Received 16 August 2011
Received in revised form 3 October 2011
Accepted 5 October 2011
Available online 10 October 2011

Keywords:
Foaming agent
Electrocatalysis
Methanol oxidation
Fuel cells
Carbon nanotubes
Nitrogen-doping

ABSTRACT

An exceptionally durable and highly active Pt catalyst has been prepared by embedding Pt nanoparticles inside the pores of a nitrogen-doped porous carbon layer coated on carbon nanotubes (denoted as Pt@NC-CNT). The aforementioned material, under different carbonization temperatures, is characterized by transmission electron microscopy, N_2 adsorption and desorption isotherms, X-ray photoelectron spectroscopy, and Raman spectroscopy. The maximum current density (I_{max}) during the methanol oxidation reaction (MOR) observed for Pt@NC-CNT (13.2 mA cm^{-1}) is 20% higher than that of the commercial Pt/XC-72 (10.8 mA cm^{-1}) catalyst. In the accelerated durability test, the I_{max} after 2000 cycles for Pt@NC-CNT-600 decreased from 13.2 to 6.9 mA cm^{-2} (48% decreased) compared with Pt/XC-72, which showed a decrease from 10.8 to 0.46 mA cm^{-2} (96% decreased). This indicates that the Pt@NC-CNT catalyst has extremely stable electrocatalytic activity for MOR owing to its unique structure, whereby Pt is protected by being embedded inside the pores of the nitrogen-doped carbon layer. Pt@NC-CNT's superior durability properties are further verified by observing the changes of the Pt particle sizes using TEM images before and after accelerated durability tests, as compared with Pt/XC-72.

1. Introduction

Porous, graphitic carbon materials have several appealing physical properties, such as low density, large surface area, high chemical inertness and thermal stability, that exhibit promising potential for many applications, including their use as catalytic support [1–5]. In general, today's most frequently employed supports, carbon black and activated carbon, have poor electrical conductivity. By contrast, carbon nanotubes (CNTs) have proven to be a better support for electrocatalysts, but they exhibit poor pore development and low surface area, which leads to low dispersion and stability of the noble metal catalyst particles [6–8]. There is increasing evidence indicating that the physical and electrochemical properties of carbon materials are extremely sensitive to doping by heteroatoms [9–12]. In particular, the doping of nitrogen into carbon produced a profound effect on surface chemical activity and electron-transfer rates [13–15]. Generally, Pt-based catalysts with nitrogen-doped carbon materials as support feature enhanced catalytic activity toward methanol oxidation and oxygen reduction, which can be attributed to modifying the interaction between the Pt catalysts and carbon support [16–19]. In addition, durability of fuel cells has also been one of the major issues to be solved to realize commercialization [19–22]. The sintering and dissolution of the Pt catalyst in the cell operation condition bring about the decrease of Pt metal surface area, and hence the performance of fuel cells is significantly decreased. To improve the durability at the electrode, numerous studies have concentrated on understanding the effects of carbon supports and exploring new carbon supports [23–28].

Compared with proton exchange membrane fuel cells (PEMFCs) fed by hydrogen, direct methanol fuel cells (DMFCs) possess many advantages such as simple processing, high energy density and low operating temperature. Additionally, unlike hydrogen, methanol is an abundant, inexpensive liquid fuel that can be easily handled, stored, and transported. However, these catalysts for methanol oxidation offer much less activity and durability under fuel cell operation conditions [28–33]. In this context, we have been striving to develop a novel high nitrogen-containing carbon nanotube (NC-CNT) by using aniline as a dispersant to CNTs and as a source for both carbon and nitrogen coated on the surface of the CNTs [19]. The doped nitrogen found in the porous carbon layer not only acts as a stabilizer in preparation for small Pt particles but also enhances the catalytic activity. In recent research, we reported on the preparation of Pt catalysts embedded in the carbon layer surrounding CNTs [34]. Here, Pt particles inside NC-CNT (denoted as Pt@NC-CNT) are protected by being embedded within the porous nitrogen-doped carbon layer, resulting in high durability.

In this paper, we elucidate the production of catalysts for methanol oxidation reactions using Pt@NC-CNT under different carbonization temperatures. The novel catalyst was then

* Corresponding author. Tel.: +886 6 275 7575×62658; fax: +886 6 2762331.
E-mail address: plkuo@mail.ncku.edu.tw (P.-L. Kuo).

0378-7753/$ – see front matter © 2011 Elsevier B.V. All rights reserved.
doi:10.1016/j.jpowsour.2011.10.012

characterized by various techniques such as transmission electron microscopy (TEM), high-resolution transmission electron microscopy (HR-TEM), N_2 adsorption and desorption isotherms, X-ray photoelectron spectroscopy (XPS), and Raman spectroscopy. Such extensive characterizations help in gaining a better understanding of the properties of the nitrogen-doped carbon layer. Furthermore, the enhanced catalytic activity and durability of the carbon-supported catalysts are also investigated and compared with commercially available catalyst.

2. Experimental

2.1. Synthesis of Pt nanoparticles embedded in nitrogen-doped porous carbon layers surrounding CNTs

The composites were synthesized by chemical oxidation polymerization of aniline on CNTs (Multi-wall carbon nanotubes, Scientech Corporation, purity ≥95%). A 20.0 mL solution of isopropyl alcohol (J.T. Baker, 99%) containing treated CNT 0.050 g was first stirred before the synthesis, followed by the addition of 0.10 g aniline monomers (Sigma–Aldrich, 99.5%) in 10 mL 0.5 M H_2SO_4 into the CNT suspension. The above solution was further mixed with 10.0 g of 0.1 M $NaOH_{(aq)}$ containing an appropriate amount of foaming agent (EDTA, Sigma–Aldrich, >99%) and 1.6 mL of Pt solution (Umicore, $H_2PtCl_6{\cdot}6H_2O$, 0.082 M) (the molar ratio of foaming agent to Pt was 1:1). The resulting mixture were subsequently stirred for 3 h at room temperature, at which point a solution of 0.50 M H_2SO_4 containing the oxidant $(NH_4)_2S_2O_8$ (ammonium peroxodisulphate, APS) was added (the molar ratio of APS to aniline was 0.8:1). Polymerization was then carried out at room temperature for 20 h. The resulting products were filtered and washed with deionized water, and then dried under vacuum at 70 °C overnight. The hybrid carbon materials were treated at different temperatures (500, 600, 650, and 800 °C) in an argon gas flow oven (100 sccm) for 3 h to form a nitrogen-doped char layer surrounding the CNTs. Then a sufficient amount of sodium borohydride was added to the mixture (the molar ratio of sodium borohydride to Pt was 15:1) and stirred for 6 h, after which it was filtered and dried in vacuum at 70 °C overnight. Finally, the sample was heated at 400 °C in a quartz-tube furnace with flowing argon gas for 2 h. The resultant products are denoted as Pt@NC-CNT-*x*, where *x* is the pyrolysis temperature (°C).

2.2. Sample characterization

The TEM portion of the study was conducted using a Hitachi-H7500 with an accelerating voltage of 80 kV. HR-TEM analysis was performed using Philips/FEI Tecnai 20 G2 S-Twin electron microscope, operated at 200 kV. Specific surface areas of the prepared catalysts were determined using the Braunauer–Emmett–Teller (BET) method on a Micromeritics ASAP 2020 instrument. XPS measurements were carried out with a VG Scientific ESCALAB 210 electron spectrometer using Mg Kα radiation under a vacuum of 2×10^{-8} Pa. Thermogravimetry (TG) analysis was performed on a thermogravimetric analyzer (TGA Q-50) over a temperature range of 50–800 °C at a heating rate of 20 °C min^{-1}. A micro Raman spectrometer from Renishaw with a He–Ne laser source with a wavelength of 633 nm was used to determine the structure of CNTs.

2.3. Electrochemical measurements

A CHI-608A potentiostat/galvanostat and a conventional three-electrode test cell were used for electrochemical measurement. GC disk electrode (5 mm diameter, Pine) served as the substrate for the supported catalyst. An aliquot of catalyst suspension was transferred onto the carbon substrate, leading to a catalyst loading of 50.9 μg catalyst cm^{-2} for Pt@NC-CNT and commercial Pt/XC-72 catalyst (E-TEK). The CV test was performed on the working electrode by cycling the voltage between −0.23 and 1.0 V versus Ag/AgCl electrode in 0.1 M $HClO_4$ solution. Electrooxidation of MeOH was carried out with an electrolyte of 0.5 M H_2SO_4 and 1.0 M MeOH between 0 and 0.95 V at room temperature. The scan rate was 20 mV s^{-1}.

3. Results and discussion

3.1. Structural properties of Pt@NC-CNT catalysts

The Pt@NC-CNT catalysts were synthesized using our previously reported method [34]. In the preparation, aniline was used to form polyaniline, which was then pyrolyzed into the nitrogen-doped porous carbon layer surrounding the CNTs, and employed to stabilize Pt^{4+} and/or Pt^0 during the reduction and pyrolysis process. The microstructure of the Pt@NC-CNT catalyst was characterized by the representative HR-TEM images shown in Fig. 1a. The images demonstrate that Pt particles are found to be surrounded by many small lines, corresponding to microporous graphitic carbon layers, which illustrates that the Pt nanoparticles are embedded within the carbon layer. In contrast to the image of Pt@NC-CNT, the image of the catalyst without using the foaming agent to chelate platinum ions (Pt@NC-CNT-*y*) (Fig. 1b) illustrates that Pt nanoparticles surrounded by amorphous nanostructures are clearly seen. The Pt@NC-CNT-*y* contains more curvature and dislocations in the structure, which is likely due to the propensity of substituted nitrogen to form pentagonal defects in the structure. Comparing the surface areas of Pt@NC-CNT and Pt@NC-CNT-*y* shows that Pt@NC-CNT (271 m^2 g^{-1}) has a significantly higher BET surface area than that of Pt@NC-CNT-*y* (120 m^2 g^{-1}). For Pt@NC-CNT, the introduction of the foaming agent into the polyaniline resulted in a 150% increase in surface area. Moreover, the electron conductivity in electrocatalysis would benefit from the layers of graphitic carbon nanostructures due to their high crystallinity, as illustrated by HR-TEM images.

The binding energy between Pt atoms and the nitrogen group on the surface of the Pt@NC-CNT and Pt@NC-CNT-*y* was characterized by XPS, as shown in Fig. 2. In the N1s region (Fig. 2a), both Pt@NC-CNT and Pt@NC-CNT-*y* show two comparable peaks at 398.6 and 400.6 eV, which are assigned to pyridinic and graphitic-type nitrogen atoms doped at the edges and in-between the graphitic carbon layers, respectively [15,35,36]. It is clear that Pt@NC-CNT contains large percentages of pyridinic nitrogen, which have been reported to be responsible for the active sites. In the Pt 4f region (Fig. 2b), the Pt 4f line shows two pairs of peaks from the spin-orbital splitting of the $4f_{7/2}$ and $4f_{5/2}$ [37,38]. The most intense doublets observed at 71.4 and 74.8 eV are attributed to zero-valent platinum Pt^0 for Pt@NC-CNT. The lower shift (0.6 eV) in binding energy observed for Pt@NC-CNT as compared to Pt@NC-CNT-*y* (72.0 eV and 75.2 eV) indicates that introducing the foaming agent caused more platinum surface to be exposed, resulting in a higher degree of reduction of the platinum catalyst. The above results suggest that the foaming agent not only leads to a high porous, high surface area carbon layer, but also exposes greater amount of platinum catalyst.

3.2. Structural properties of Pt@NC-CNT catalyst under different carbonization temperatures

To study the effects carbonization temperature on the particle size of Pt@NC-CNT catalysts, TEM images were compared, as in Fig. 3. Without carbonization (Fig. 3a), the CNT surface is coated by polyaniline, with the platinum ions encapsulated inside the polyaniline. In the low temperature carbonization process (500 °C,

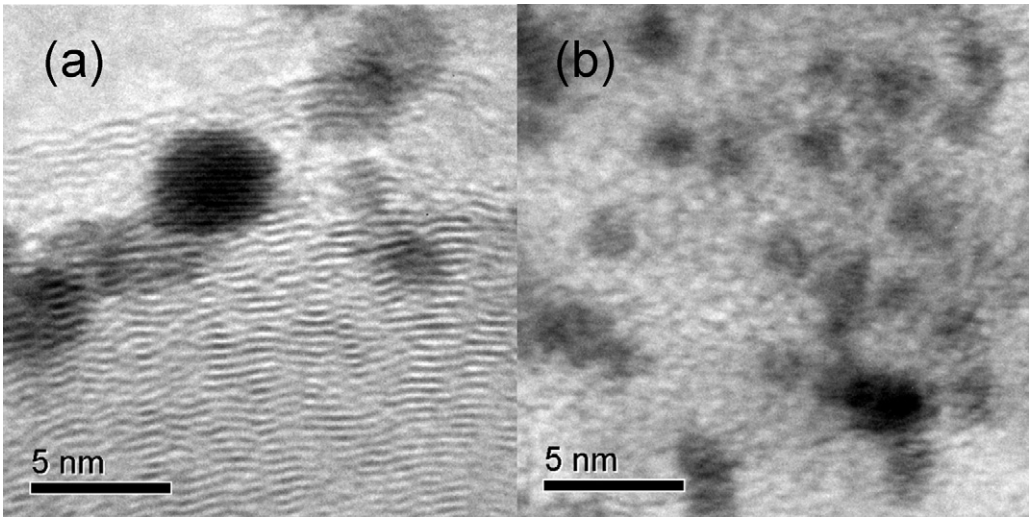

Fig. 1. HR-TEM images of (a) Pt@NC-CNT and (b) Pt@NC-CNT-*y*.

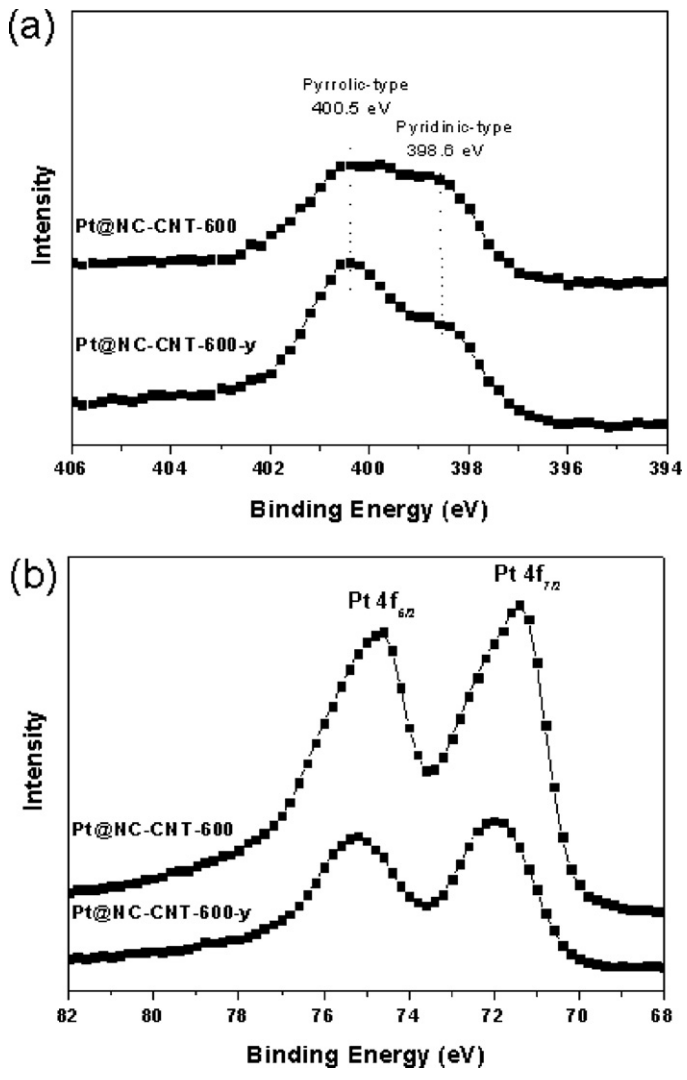

Fig. 2. The XPS spectra of Pt@NC-CNT and Pt@NC-CNT-*y* catalysts at (a) N_{1s} and (b) Pt 4_f regions.

Fig. 3b), polyaniline began to dehydrogenate and partially denitrogenate to form a carbon layer surrounding the CNT. In the pyrolysis process, most of the foaming agent pyrolyzed into gas which was blown away in the tubular furnace by carrier gas ($Ar_{(g)}$), with residual foaming agent being reduced to less than 10 wt%. As the foaming agent gasified, Pt became exposed and reduced, resulting in the size of the Pt catalyst being about 1.2 ± 0.5 nm. At higher pyrolysis temperatures (600 and 650 °C, Fig. 3c and d), the thickness of the carbon layer began to decrease while the size of the Pt catalyst increased to 2.8 ± 1.1 and 3.1 ± 1.1 nm, respectively. When the carbonization temperature was increased to 800 °C (Fig. 3e), the Pt catalyst significantly increased in size (4.9 ± 2.6 nm) and aggregated seriously. These observations show that particle size variation is significantly influenced by the increasing carbonization temperature. In comparison, it can be seen from the TEM image of the Pt@NC-CNT-600-*y* catalyst, which is produced without using the foaming agent (Fig. 3f), that the size of Pt particles is smaller (1.6 ± 0.3 nm) and more uniform than Pt@NC-CNT-600. This means that bubbles induced by the gas generator create more space to allow for the coagulation of Pt under high temperature.

The textural properties of Pt@NC-CNT obtained after different carbonization temperatures (Pt@NC-CNT-*x*) were further characterized by measuring the nitrogen adsorption–desorption isotherms. The structural properties of various Pt@NC-CNT-*x* are summarized in Table 1. As shown in Fig. 4, the entire Pt@NC-CNT-*x* sample generally exhibited the typical type-IV isotherms, suggesting the existence of mesopores in the samples [37]. Upon further increasing the pyrolysis temperature, the hysteresis loops for the samples became more prominent. Additionally, the abrupt increases in adsorption/desorption curves observed for Pt@NC-CNT-*x*, occurring at a higher relative pressure ($P/P_o > 0.90$), could be attributed to condensation of N_2 in the center and in interparticle voids of the sample. That a higher surface area was observed for Pt@NC-CNT-650 ($214\ m^2\ g^{-1}$) than the Pt@NC-CNT-500 ($151\ m^2\ g^{-1}$) indicates that no substantial carbonization of the polyaniline shell took place at a pyrolysis temperature of 500 °C. However, upon increasing the pyrolysis temperature from 650 to 800 °C, the surface area of Pt@NC-CNT-*x* was slightly decreased from 214 to $202\ m^2\ g^{-1}$. This trend is consistent with the results of Raman spectroscopy (discussed below).

The electrical conductivity of the Pt@NC-CNT-*x* was further characterized by four-point probe method, also shown in Table 1. The pristine CNTs exhibited an electrical conductivity of $149.2\ S\ cm^{-1}$ and the electrical conductivity of Pt@NC-CNT-500,

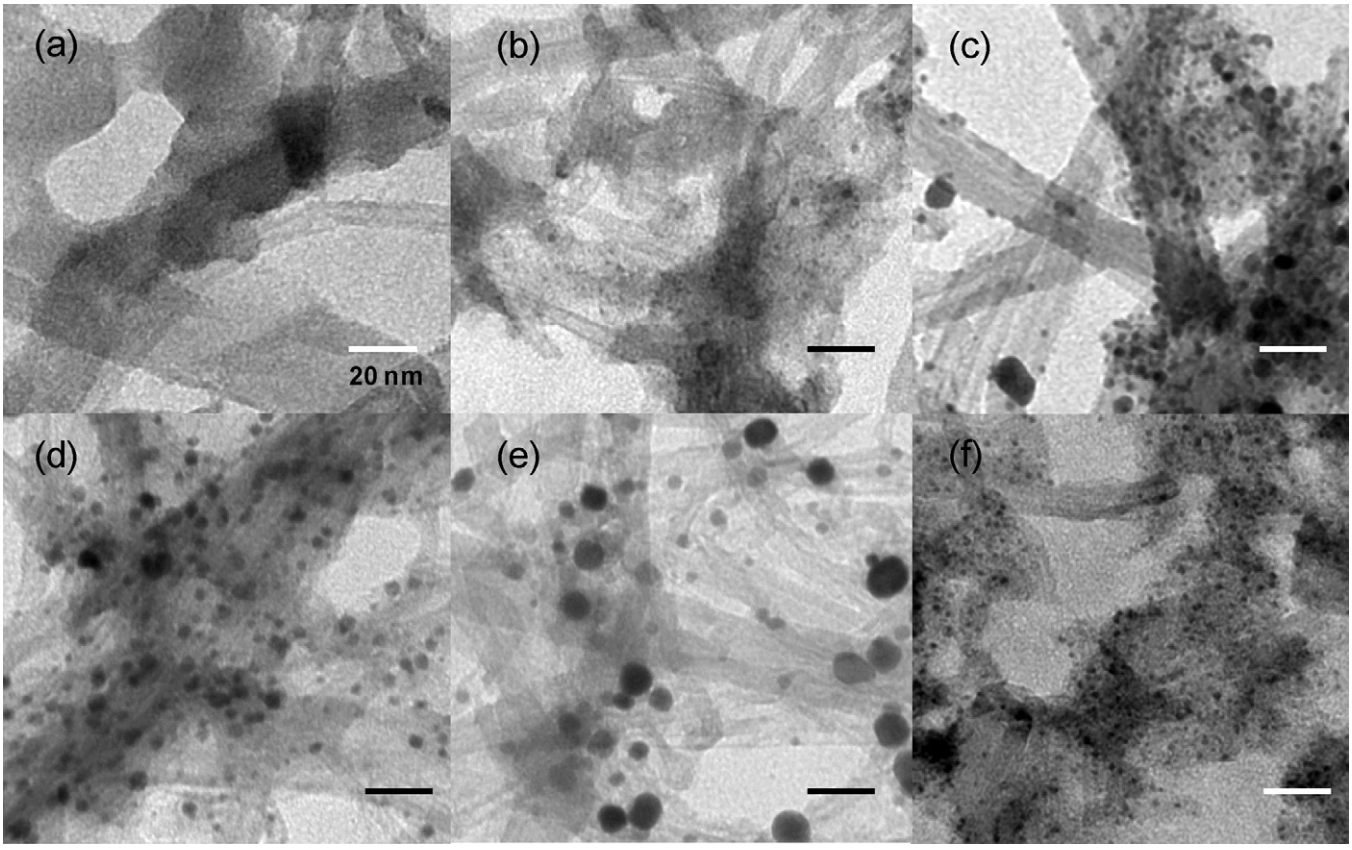

Fig. 3. TEM images of (a) Pt@polyaniline/CNT, (b) Pt@NC-CNT-500, (c) Pt@NC-CNT-600, (d) Pt@NC-CNT-650, (e) Pt@NC-CNT-800 and (f) Pt@NC-CNT-600-*y* catalysts.

Table 1
Structure parameter of various Pt@NC-CNT catalysts.

Sample	Particle size[a] (nm)	S_{BET}[b] ($m^2\ g^{-1}$)	S_{Micro}[c] ($m^2\ g^{-1}$)	S_{Meso}[c] ($m^2\ g^{-1}$)	V_{total}[b] ($cm^3\ g^{-1}$)	Conductivity[d] ($S\ cm^{-1}$)
Pt@NC-CNT-500	1.2 ± 0.5	151	83	68	0.34	30.1
Pt@NC-CNT-600	2.8 ± 1.1	271	60	211	0.58	32.6
Pt@NC-CNT-650	3.1 ± 1.1	242	54	188	0.41	48.5
Pt@NC-CNT-800	4.8 ± 2.6	202	37	165	0.36	81.3
Pt@NC-CNT-600-*y*	1.4 ± 0.3	120	24	96	0.35	35.2

[a] Pt particle size measured by the TEM images.
[b] BET surface area and total pore volume obtained from the N_2 adsorption/desorption isotherms.
[c] Microporous and mesoporous surface area obtained from the *t*-plot analyses.
[d] Conductivity were measured by four-point probe.

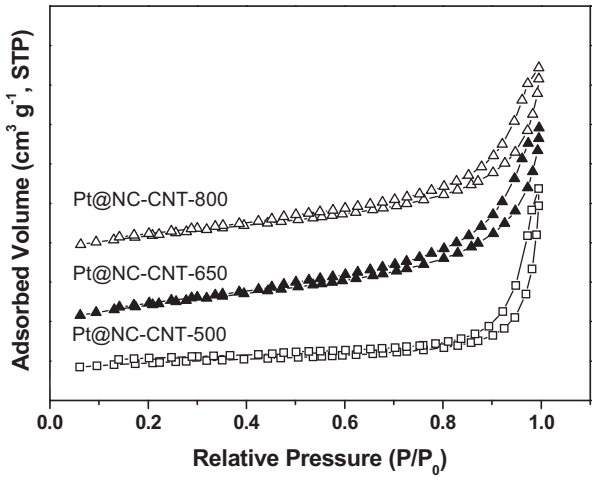

Fig. 4. N_2 adsorption/desorption isotherms of various Pt@NC-CNT-*x*.

Pt@NC-CNT-600, Pt@NC-CNT-650 and Pt@NC-CNT-800 are 30.1, 32.6, 48.5, and 81.3 S cm^{-1}, respectively. Evidently, the amorphous carbon char on CNT resulted a decrease in electrical conductivity, however, due to the CNT-base core, the electrical conductivity of NC-CNT is better than that of commercial carbon support XC-72 (29.2 S cm^{-1}). This reveals that the carbon layer on CNT enable the conduction of electrons among carbon nanotubes more effectively than XC-72.

Nitrogen doping via the replacement of C atoms with N atoms has been confirmed by XPS as mentioned above, after which the effects of nitrogen doping on the carbon graphitic structures and crystallinity were further investigated using Raman spectroscopy (Fig. 5) as follows. Pristine CNTs exhibit two main characteristic absorptions: G-band (~1580 cm^{-1}) is assigned to the in-plane displacement of carbon atoms in the hexagonal sheets, and D-band (~1350 cm^{-1}) is due to the disorder of the structure [28]. The extent of the defects in carbon materials can be quantified by the intensity ratio of D to G bands (i.e., I_D/I_G). The I_D/I_G ratios are 1.02, 0.86, and 0.93 for Pt@NC-CNT-500, Pt@NC-CNT-650 and

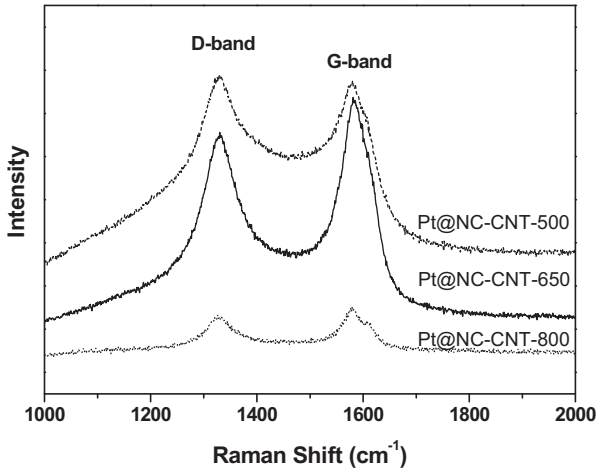

Fig. 5. Raman spectroscopy of various Pt@NC-CNT-*x*.

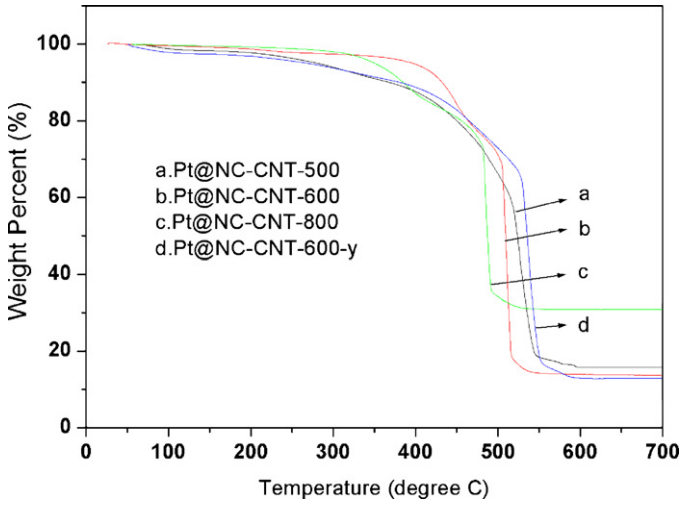

Fig. 6. TGA curves of various Pt@NC-CNT-*x*, recorded in air stream.

Pt@NC-CNT-800, respectively. Again, the results show that lower defects were observed for Pt@NC-CNT-650 than Pt@NC-CNT-500. This is an indication that no substantial carbonization of the polyaniline shell took place at a pyrolysis temperature of 500 °C, while the defects of Pt@NC-CNT-*x* slightly increased with an

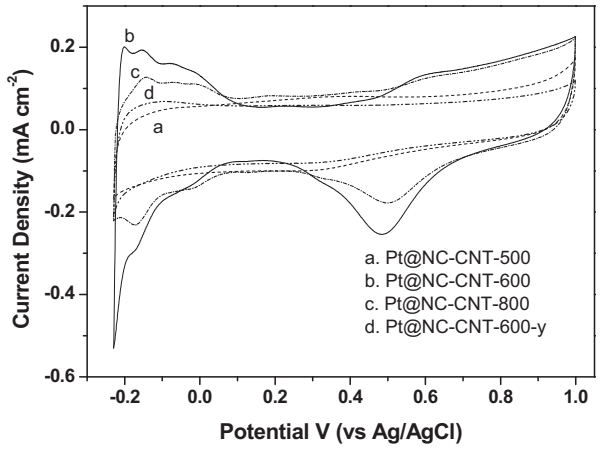

Fig. 7. The CV curves of various Pt@NC-CNT-*x* in 0.1 M $HClO_{4(aq)}$ at a scan rate of 20 mV s^{-1}.

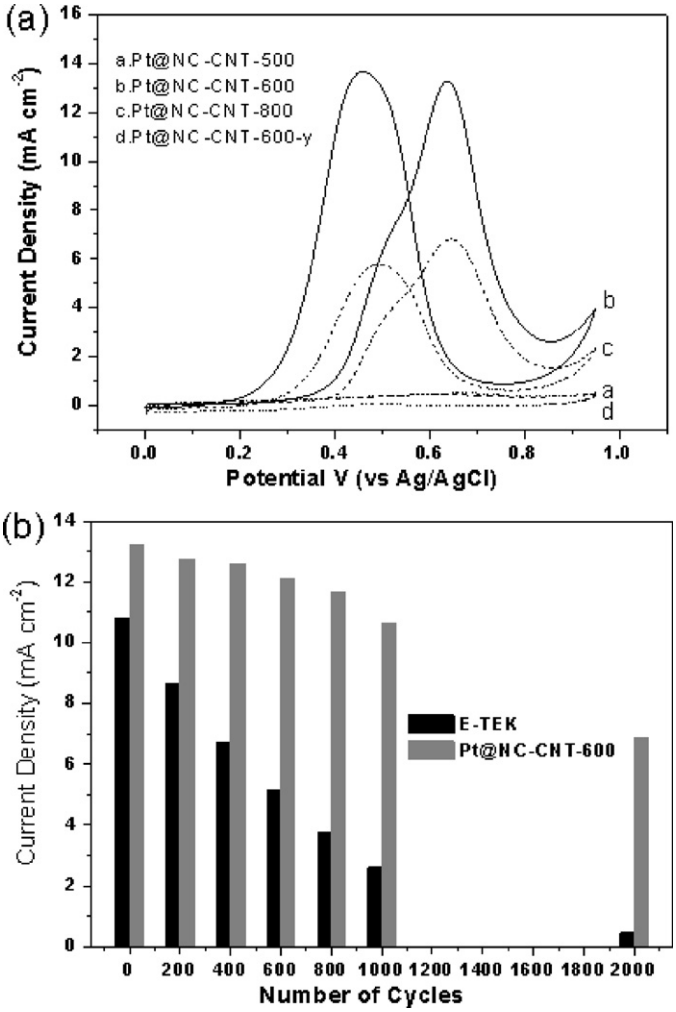

Fig. 8. The CV curves of various Pt@NC-CNT-*x* in (a) 1.0 M MeOH + 0.5 M $H_2SO_{4(aq)}$ at a scan rate of 20 mV s^{-1}. (b) Accelerated durability tests.

increase in the pyrolysis temperature from 650 to 800 °C. This trend is consistent with the TEM results shown in Fig. 3, where the aggregation of platinum has induced severe destruction of the carbon structure. Such structural damage of the carbon layers is accompanied by decreases in the surface area and electrical conductivity of the carbon support.

Fig. 6 shows the TGA curves of the Pt@NC-CNT-500, Pt@NC-CNT-600, Pt@NC-CNT-800 and Pt@NC-CNT-600-*y*, recorded in air stream. There are three apparent decreases in the sample weights shown in the thermograms. The first step ranged from 50 to 150 °C and was attributed to the evaporation of the hydration water. A second apparent weight loss was produced between 250 and 500 °C and was attributed to the decomposition of polyaniline. Above 500 °C, there was an appreciable loss of mass, which corresponds to the decomposition of CNT and high crystalline carbon. Furthermore, the real loading percentages of Pt in the Pt@NC-CNT composites were analyzed by measuring the residual percentages as shown in Table 2. The result shows that higher carbonization temperature, the lower thermal stability of Pt@NC-CNT-*x* composite. This result may be due to higher weight loss of polyaniline/CNT composite under higher carbonization temperature (ex. Pt@NC-CNT-800), while the weight percentage of catalyst is relatively increased, making the lower thermal stability of product. In addition, both Pt@NC-CNT (13.7%) and Pt@NC-CNT-*y* (12.8%) show similar Pt loading percentage. The lower thermal stability observed for Pt@NC-CNT as compared to Pt@NC-CNT-*y* (decomposition of

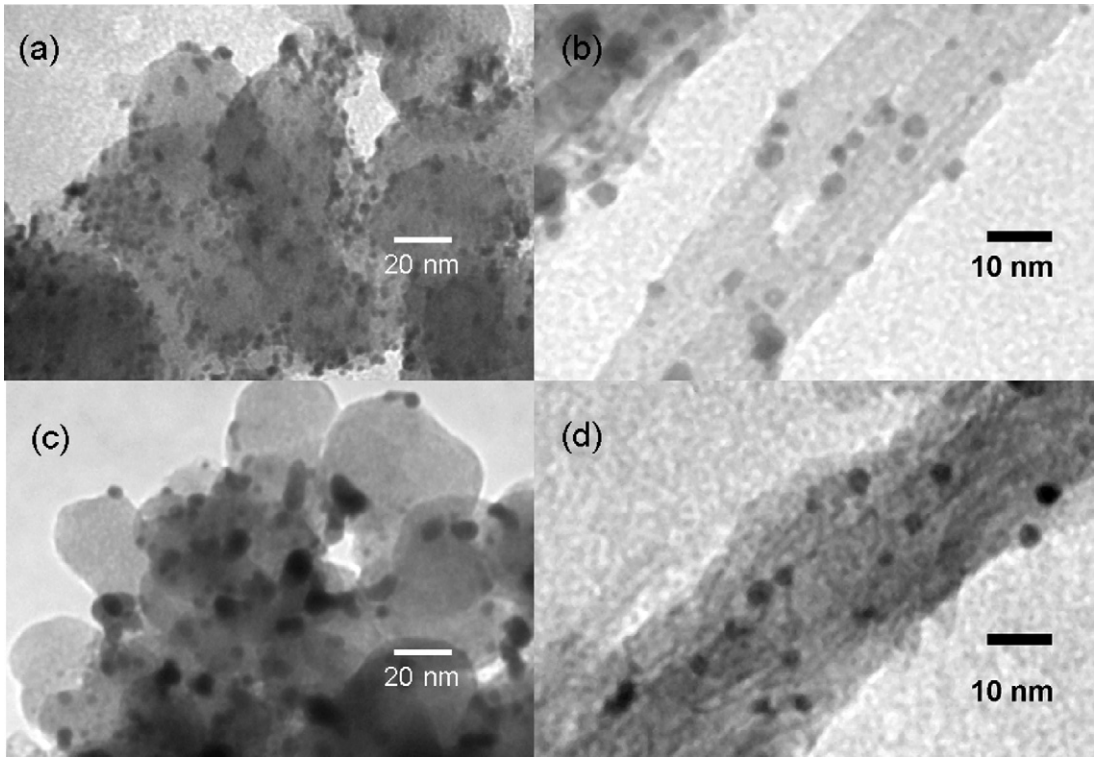

Fig. 9. TEM images of the (a, c) E-TEK and (b, d) Pt@NC-CNT-600 catalysts (a, b) before and (c, d) after 2000 potential cycles.

CNT at 505 and 535 °C, respectively) indicates that introducing the foaming agent caused more Pt surface to be exposed, resulting in a higher activity of the Pt catalyst.

3.3. Electrocatalytic activity for methanol oxidation reaction

To illustrate how the nitrogen-doped shell on the CNT affects the electrochemical properties of embedded Pt in NC-CNT, the electrochemically active surface areas (EAS) were measured. The EAS was estimated by the integrated charge (after excluding the double layer charging effect) in the hydrogen adsorption–desorption region (from −0.2 to 0.1 V using Ag/AgCl as reference). For the cyclic voltammograms (CV) of the Pt/C catalyst (Fig. 7), the EAS was 64 $m^2 g^{-1}$ for Pt@NC-CNT-600 and 1.3 $m^2 g^{-1}$ for Pt@CNT-600-*y*. The lower EAS value of Pt@NC-CNT-600-*y* can be attributed to the covered Pt particles. The higher EAS value of Pt@NC-CNT-600 is likely induced by the Pt particle surface being separated from the N-doped carbon char, thereby becoming more exposed, and caused by the foaming agent being pyrolyzed. Furthermore, the EAS values are similar to that of E-TEK (68 $m^2 g^{-1}$), despite the embedded Pt nanoparticles. To further explore the effect of different carbonization temperatures, the EAS for Pt@NC-CNT-500 (<10 $m^2 g^{-1}$) is smaller than Pt@NC-CNT-600 (64 $m^2 g^{-1}$). Again, the high temperature decomposition of polyaniline enables greater exposure of Pt to hydrogen, and therefore exhibits more activity. However, with a further increase in carbonization temperature, the EAS became 22 $m^2 g^{-1}$ for Pt@NC-CNT-800. This is consistent with the TEM results shown in Fig. 1, where the aggregation of platinum caused a larger particle size accompanied with low EAS and electrochemical activity.

Table 2
Electrochemical parameters and catalytic performances of various Pt@NC-CNT catalysts during methanol oxidation reaction.

Sample	Pt content (%)[a]	EAS ($m^2 g^{-1}$)	I_{max} ($mA cm^{-2}$)
Pt@NC-CNT-500	15.8%	<10	0.6
Pt@NC-CNT-600	13.7%	64	13.2
Pt@NC-CNT-800	30.8%	22	6.8
Pt@NC-CNT-600-*y*	12.8%	<10	0.51
E-TEK	20%	68	10.8

[a] Total Pt loading (wt%) was quantified by TGA.

Typical voltammetric curves for methanol oxidation of Pt@NC-CNT catalysts in N_2 saturated 0.5 M H_2SO_4 and 1.0 M MeOH aqueous solution is shown in Fig. 8a. The maximum current density (I_{max}) during methanol oxidation was measured from voltammetric curves for Pt@NC-CNT-600 (13.2 $mA cm^{-2}$), Pt@NC-CNT-600-*y* (0.51 $mA cm^{-2}$) and Pt/XC-72 electrode (10.8 $mA cm^{-2}$), as shown in Table 2. For Pt@NC-CNT-600-*y*, the low value in maximum current density corresponds to its low EAS. In contrast to Pt@NC-CNT-600-*y*, Pt@NC-CNT-600 showed a 25-times higher value than Pt@NC-CNT-600-*y* in catalytic activity due the surface of the Pt nanoparticles being more exposed, correlating with the results of the EAS. This further suggests that the function of the foaming agent used for preparing Pt@NC-CNT in this novel synthesis technique is of paramount importance to the catalytic ability of the methanol oxidation reaction (MOR). Furthermore, both the I_{max} for Pt@NC-CNT-500 (0.6 $m^2 g^{-1}$) and Pt@NC-CNT-800 (6.8 $m^2 g^{-1}$) are smaller than Pt@NC-CNT-600, corresponding to their low EAS values.

The electrocatalyst durability of the Pt@NC-CNT and of Pt/XC-72 were evaluated through repeated CV cycles with the appropriate lower and upper potential limits in a 0.5 M H_2SO_4 and 1.0 M MeOH solution. After 2000 cycles, the I_{max} of MOR for Pt@NC-CNT (6.9 $mA cm^{-2}$) was 15 times higher than that of E-TEK (0.46 $mA cm^{-2}$) (Fig. 8b). This means that the Pt@NC-CNT catalyst has extremely stable electrocatalytic activity for MOR owing to the unique structure of Pt@NC-CNT, where Pt is protected by being embedded inside the porous N-doped carbon char. This result was confirmed by observing the changes in the Pt particle sizes of both

catalysts before and after the accelerated durability test using the TEM images, as shown in Fig. 9a and c. The particle size of the E-TEK (Pt/XC-72) catalyst increased from 2.8 nm to larger than 10 nm after the durability test. Here, the main reason for the decrease in the current density of MOR of Pt/XC-72 was confirmed to be the sintering of the Pt particles as evidenced from the TEM images. On the other hand, the TEM image of the Pt@NC-CNT catalyst shows a similar particle size before and after the durability test, as shown in Fig. 9b and d. Again, we can conclude that the unique structure of Pt@NC-CNT provides extremely high catalytic durability, where the embedded Pt within the porous carbon char is likely protected to prevent agglomeration of Pt particles in the carbon support.

4. Conclusion

The particle size variation of Pt@NC-CNT is significant with respect to an increasing carbonization temperature. The HR-TEM, surface area, and XPS results show that adding the foaming agent not only encourages high porosity forms and a large carbon-layer surface area, but also exposes more of the platinum catalyst, resulting in a higher degree of platinum catalyst reduction. In the durability test, after 2000 cycles, the I_{max} for MOR was 0.46 and 6.9 mA cm^{-2} for Pt/XC-72 and Pt@NC-CNT, respectively. Moreover, the Pt@NC-CNT catalyst has extremely stable electrocatalytic activity for MOR owing to its unique structure, where Pt is protected by being embedded inside the porous N-doped carbon char.

Acknowledgments

The authors would like to thank the National Science Council, Taipei, ROC for their generous financial support of this research, Professor Hong-Ping Lin for HR-TEM images, TGA and nitrogen adsorption and desorption isotherms.

References

[1] J.H. Kim, B. Fang, S.B. Yoon, J.S. Yu, Appl. Catal. B: Environ. 88 (3–4) (2009) 368–375.
[2] G. Girishkumar, K. Vinodgopal, P.V. Kamat, J. Phys. Chem. B 108 (52) (2004) 19960–19966.
[3] G. Wu, D.Y. Li, C.S. Dai, D.L. Wang, N. Li, Langmuir 24 (7) (2008) 3566–3575.
[4] J.S. Yu, S. Kang, S.B. Yoon, G. Chai, J. Am. Chem. Soc. 124 (32) (2002) 9382–9383.
[5] Z.H. Wen, J. Liu, J.H. Li, Adv. Mater. 20 (4) (2008) 743–747.
[6] C. Song, J.P. Du, J.H. Zhao, S.A. Feng, G.X. Du, Z.P. Zhu, Chem. Mater. 21 (8) (2009) 1524–1530.
[7] H.S. Liu, C.J. Song, L. Zhang, J.J. Zhang, H.J. Wang, D.P. Wilkinson, J. Power Sources 155 (2) (2006) 95–110.
[8] W.L. Xu, X.C. Zhou, C.P. Liu, W. Xing, T.H. Lu, Electrochem. Commun. 9 (5) (2009) 1002–1006.
[9] C.W.B. Bezerra, L. Zhang, K.C. Lee, H.S. Liu, A.L.B. Marques, E.P. Marques, et al., Electrochim. Acta 53 (15) (2008) 4937–4951.
[10] S. Maldonado, K.J. Stevenson, J. Phys. Chem. B 109 (10) (2005) 4707–4716.
[11] P.H. Matter, E. Wang, M. Arias, E.J. Biddinger, U.S. Ozkan, J. Phys. Chem. B 110 (37) (2006) 18374–18384.
[12] F. Charreteur, F. Jaouen, S. Ruggeri, J.P. Dodelet, Electrochim. Acta 53 (6) (2008) 2925–2938.
[13] P. Wang, Z.Y. Ma, Z.C. Zhao, L.X. Ha, J. Electroanal. Chem. 611 (1-2) (2007) 87–95.
[14] R.A. Sidik, A.B. Anderson, J. Phys. Chem. B 110 (4) (2006) 1787–1793.
[15] Z. Lei, M. Zhao, L. Dang, L. An, M. Lu, A.Y. Lo, et al., J. Mater. Chem. 19 (33) (2009) 5985–5995.
[16] K. Gong, F. Du, Z. Xia, M. Durstock, L. Dai, Science 323 (5915) (2009) 760–763.
[17] C.V. Rao, C.R. Cabrera, Y. Ishikawa, J. Phys. Chem. Lett. 1 (18) (2010) 2622–2627.
[18] G. Vijayaraghavan, K.J. Stevenson, Langmuir 23 (10) (2007) 5279–5282.
[19] C.H. Hsu, H.M. Wu, P.L. Kuo, Chem. Commun. 46 (40) (2010) 7628–7630.
[20] Y.C. Hsieh, J.Y. Chen, P.W. Wu, J. Power Sources 196 (20) (2011) 8225–8233.
[21] Y. Yuan, J.A. Smith, G. Goenaga, D.j. Liu, Z.P. Luo, J.B. Liu, J. Power Sources 196 (15) (2011) 6160–6167.
[22] Y.G. Chen, J.J. Wang, H. Liu, M.N. Banis, R.Y. Li, X.L. Sun, et al., J. Phys. Chem. C 115 (9) (2011) 3769–3776.
[23] X. Wang, W.Z. Li, Z.W. Chen, M. Waje, Y.S. Yan, J. Power Sources 158 (1) (2006) 154–159.
[24] Y.Y. Shao, G.P. Yin, Y.Z. Gao, P.F. Shi, J. Electrochem. Soc. 153 (6) (2006) A1093–A1097.
[25] Y.Y. Shao, G.P. Yin, J. Zhang, Y.Z. Gao, Electrochim. Acta 51 (26) (2006) 5853–5857.
[26] Y.Y. Shao, S. Zhang, C.M. Wang, Z.M. Nie, J. Liu, Y. Wang, et al., J. Power Sources 195 (15) (2010) 4600–4605.
[27] J.J. Wang, G.P. Yin, Y.Y. Shao, Z.B. Wang, Y.Z. Gao, J. Power Sources 112 (15) (2008) 5784–5789.
[28] P.L. Kuo, C.H. Hsu, W.T. Li, J.Y. Jhan, W.F. Chen, J. Power Sources 195 (24) (2010) 7983–7990.
[29] S.H. Liu, W.Y. Yu, C.H. Chen, A.Y. Lo, B.J. Hwang, S.H. Chien, et al., Chem. Mater. 20 (4) (2008) 1622–1628.
[30] B. Lim, M. Jiang, P.H.C. Camargo, E.C. Cho, J. Tao, X. Lu, et al., Science 324 (5932) (2009) 1302–1305.
[31] J. Zhang, K. Sasaki, E. Sutter, R.R. Adzic, Science 315 (5809) (2007) 220–222.
[32] D.H. Lim, W.D. Lee, D.H. Choi, H.I. Lee, Appl. Catal. B: Environ. 94 (1–2) (2010) 85–96.
[33] F. Wen, U. Simon, Chem. Mater. 19 (14) (2007) 3370–3372.
[34] P.L. Kuo, C.H. Hsu, ACS Appl. Mater. Interfaces 3 (2) (2011) 115–118.
[35] B. Choi, H.S. Yoon, I.S. Park, J.S. Jang, Y.E. Sung, Carbon 45 (2007) 2469–2501.
[36] W.J. Gammon, O. Kraft, A.C. Reilly, B.C. Holloway, Carbon 41 (10) (2003) 1917–1923.
[37] C.H. Hsu, H.Y. Liao, P.L. Kuo, J. Phys. Chem. C 114 (2010) 7933–7939.
[38] P.L. Kuo, W.F. Chen, C.Y. Lin, J. Power Sources 194 (2009) 234.